Quantitative Measurements of the Critical Impeller Speed for Solid-Liquid Suspensions

Alberini, Federico

DOI:
10.1002/ceat.201800716

Document Version
Peer reviewed version

Citation for published version (Harvard):
Alberini, F 2019, 'Quantitative Measurements of the Critical Impeller Speed for Solid-Liquid Suspensions', *Chemical Engineering & Technology*, vol. 42, no. 8, pp. 1643-1653. https://doi.org/10.1002/ceat.201800716

Quantitative measurements of critical impeller speed for solid/liquid suspensions

Guichuan Ye[1,2], Alvin W Nienow[1], Federico Alberini[1]*
[1]School of Chemical Engineering, University of Birmingham, B15 2TT, UK
[2]School of Chemical & Environmental Engineering, China University of Mining & Technology (Beijing), 100083, China
*Correspondence: Federico Alberini (E-mail: F.Alberini@bham.ac.uk), School of Chemical Engineering, University of Birmingham, B15 2TT, UK

Abstract

Particle suspension is an important consideration in stirred tanks. To date, the most used methodology to evaluate the solid suspension has largely relied on human visual observation. This method implies potentially high errors on the measurements and it is influenced by human subjectivity. In this study, a new quantitative methodology for particle suspension assessment is presented. A new parameter, $f_{mov/tot}$, is introduced to evaluate the minimum speed required to just suspend solids (N_{js}). This methodology has been tested to investigate the impact of impeller clearance on N_{JS} in a flat baffled vessel when using a radial flow Rushton turbine. Flow patterns and power numbers obtained experimentally and computationally are also used to support the suspension findings. Results show that the image analysis method is an appropriate method for determining N_{js}. Lowering the impeller clearance reduces the speed required for particle suspension with a change of flow pattern from a radial discharge with two loops to a single loop scouring the vessel base. The power number also falls markedly at the two-to-one loop transition as does the strain rate near the base. Overall, it is concluded that this new methodology allows objective measurements for the characterization of particle suspension.

Keywords: Image analysis, Impeller clearance, Particle suspension, Power number, Rushton turbines

1. Introduction

The particle suspension is one of the most important unit operations in chemical, mineral and even the new biologics industries for reactions, crystallization, and mass transfer [1-3]. Generally, the stirred tank is usually operated at the critical impeller speed, N_{js}, which is the minimum impeller speed at which no particles remain stationary at the tank bottom for more than 1 or 2 seconds [4]. Below this critical impeller speed, the total solid-liquid interfacial surface area is not efficiently utilized. Above this speed, the solid-liquid mass transfer rate increases slowly with agitation intensity [5].

During the last decades, numerous methods have been applied to quantify solid-liquid suspension performance including Positron Emission Particle Tracking (PEPT) [6], Light Sheet Image Analysis (LSIA) [7], Photo-Electric Method (PEM) [8], and Electrical Resistance Tomography (ERT) [9]. In

Received: December 12, 2018; revised: March 28, 2019; accepted: April 23, 2019

To be cited as: Chem. Eng. Technol. 10.1002/ceat.201800716

Link to final VoR: https://doi.org/10.1002/ceat.201800716

addition, Particle Image Velocity (PIV) [10, 11] and Laser Doppler Velocity (LDV) [12] were also used to measure the velocity of particles with solid concentrations below 0.2%. Other studies were focused on the measurement of N_{js}. The traditional and most common used method is the visual technique. The motion of the particles was observed through the tank bottom and N_{js} was defined as the impeller speed at which no solids remain on the tank bottom for more than 1 or 2 seconds [4]. By examining the N_{js} of a wide range of particles at different concentrations in six sizes of flat based, baffled tank with different types of the impeller, Zwietering [4] proposed a method for correlating the data using dimensional analysis. However, Ayranci and Kresta [13] critically analysed Zwietering's data treatment and reported that it was only appropriate for solids concentration up to 2 wt% solids. Other researchers concluded that N_{js} predicted by Zwietering's method was much higher than N_{js} as measured by them [14-16]. To improve the measurement for N_{js}, Tamburini et al. [17] and Jafari et al. [18] have extensively reviewed the topic and summary of experimental methods N_{js} is given in Tab. 1.

In general, although lots of effort has been put into the topic, the method for N_{js} measurement still needs to be improved. Commenting on the methods listed in Table 1, the traditional visual observation method has also been used to measure the, slurry height as a measure of particle suspension. However, it is even harder to determine the clear interface between the particles and fluid. For the solid concentration and pressure test, the main drawbacks lie in the measurement accuracy. The latest measurement method, Gamma-ray densitometry for example, faces the problem of being expensive and safety needs to be taken into consideration during the experiment. Recently, CFD methods were also used to predict N_{js}. For example, Tamburini et al. predicted N_{js} using many of the criteria in Table 1 with an Eulerian-Eulerian approach [17] but the CFD results gave very different N_{js} speeds with each criterion. Since individual particles are modeled by the latter CFD method, further effort with Lattice Boltzmann Method (LBM) [30] and Discrete Phase Method (DEM) [31, 32] were used. CFD plus DEM has also been applied for N_{js} prediction [31]. The agreement between these simulation methods was generally poor. However, this disparity seems to be reasonable because much of the complex physics of multi-particle motion in the stirred tank is ignored during simulation. Thus, modelling methods need further improvement in future.

Visual observation has generally shown that reducing the impeller clearance above the base, C, relative to the tank diameter, T, in the geometry of interest here, also reduces the speed or mean specific energy dissipation rate required to achieve suspension. Using this technique, Nienow [33] was the first to report the impact of clearance for this geometry and also showed suspension was achieved most efficiently using large impellers with small clearances. Ibrahim and Nienow provided further confirmation that the reduction of clearance changed the flow pattern and that this was associated with a fall in Po and also a lowering of N_{js} [34, 35]. Besides, Armenante and Nagamine using C/T values down to T/48 and D/T values of 0.22, 0.26 and 0.35 also noted that the biggest increase in N_{js} in conjunction with the flow pattern change

In addition to studies of particle suspension behavior in a stirred tank, the effects of impeller clearance on flow patterns have also been studied experimentally and numerically. Flow pattern transition in a stirred vessel equipped with a Rushton turbine with different impeller clearance was investigated by Montante et al. [36], using Laser Doppler anemometry (LDA). The results showed that the transition from the double to a single-loop configuration of the flow field was found to take place for C/T values between 1/7 and 1/5 [36]. Similiarly, Ochieng et al. [37] also investigated the effect of the impeller clearance on the velocity field numerically and the simulation results suggested that at a low impeller clearance, the Rushton turbine generates a flow field that evolves from the typical two loops to a single loop with an increase in downward axial flow [37]. This increase in axial flow with the single loop suggest it should be easier to suspend particles from the tank bottom. Also, Armenante and Nagamine [5, 38] reported that the larger the D/T, the lower the value of C/T at which the flow pattern change occurred.

Recently, Grenville et al. [39] developed a new approach with a theoretical analysis based on Kolmogorov's theory of homogeneous isotropic turbulence for pitched blade turbines. Grenville et al. [40] then used the same approach to analyse N_{JS} data from Chapman [41] for the current configuration of interest. Based on these data, Grenville et al. [40] found that the impact of lowering impeller clearance on N_{JS} was not statistically significant. This conclusion is so very different from the majority of the literature that it is an ideal target for assessing the new technique developed here.

The image processing method has been applied to present the particle distribution in a stirred tank [42-44]. At present, this kind of method normally used to tell the difference of particles distribution near the tank bottom. Deeper study of the information using the image processing method was paid limited attention.

The aim of the present work is to develop a new and more quantitative approach to determining the minimum conditions required for particle suspension in a stirred vessel and to use it to throw further light concerning the impact of impeller clearance in flat based vessels with Rushton turbines. This structure of the paper is such that firstly the new image processing methodology is set out. This methodology is then used to look at the effect of impeller clearance on the speed required for particle suspension. In addition, a 3D CFD simulation and 2D-PIV measurements for the single phase flow at different C/T values are undertaken. Power number is also measured and used to compare the mean specific energy dissipation rate at different impeller clearances. In addition, the new results are compared with predictions from previous studies and simultaneous visual observation. The value of the paper lies in presenting this new measurement method, its comparison with earlier literature and application to a recent disagreement in it.

2. Material and Methods: Computational and Experimental Approach

2.1. Stirred tank configuration

The experimental system consists of a 100 mm diameter cylindrical transparent tank with four equally spaced baffles and agitated by a standard six-bladed Rushton turbine impeller. The stirred tank configuration is depicted in Fig. 1 a and Tab. 2. The Rushton turbine (D/T= 1/3) was located at one of three positions (C/T = 1/3, 1/5, 1/7) for the numerical and experimental studies.

2.2. Materials

In each simulation the liquid phase had a fluid density, ρ_L, and viscosity, μ_L, 1000 kg/m^3 and 1 mPa·s respectively and in the experiments, water was used with essentially the same properties as in the simulations. As usual, Silver Coated Hollow Glass Spheres (S-HGS) tracer particles for PIV measurements with a density of 1450 kg/m^3 and of size, 10µm were used. For suspension studies, mono-dispersed glass particles were used of size, d_p = 0.5 mm and density, ρ_p = 2450 kg/m^3 at a concentration of 5% w_{solid}/w_{liquid} at different impeller clearances.

2.3. System investigated

The particle suspension performance was assessed with a novel technology as described in detail below. A schematic diagram of the CFD-simulated and experimental geometry is illustrated in Fig. 1.

Figure 1. Experimental set-up

2.3.1. Image analysis for particle suspension

To assess particle suspension performance, a quantitative measurement was developed by observing those particles at the bottom of the tank using a high speed *(HS*) camera. To determine the amount of particles unsuspended at the bottom for the different impeller clearances, the HS camera captured the cross section of the vessel. The vessel was located on top of a 45 degrees mirror and two equal source of light were used to illuminate equally the bottom of the vessel. The light beams were projected at approximatively 45 degrees from 2 sides of the vessel which were set perpendicularly to the mirror. The projected images of the bottom of the vessel on the mirror were captured with the camera. The rig set up is illustrated in Fig. 1 c. For each experiment, 2000 images were captured with the HS camera at a frequency of 2000 fps.

Figure 2. Image processing procedure

The image processing procedure is illustrated in Fig. 2. Firstly, the images were cropped to cover the area of interest (*AOI*), i.e. the tank bottom. The second step was to identify the background grey scale value which was 30. This step was done by evaluating the maximum grey scale values at the bottom of the vessel without particles.

Then, an average image was calculated from the 2000 cropped images to identify the average distribution of greyscale values at the bottom for each specific run. From this average image, the average amount of unsuspended particles ($\tilde{x}$) was obtained by calculating the number of pixel with grey scale values above the background value. Third step was to calculate the amount of moving particles from one image to the other. For this step, nine different frequencies were investigated. This step implies the use of different consecutive images for the determination of the moving particles. The images for a selected frequency (*f*) was determined from the total number of images divided by fixed time interval, which was calculated from f^{-1}.

Figure 3. New parameter $f_{mov/tot}/f_{max}$ vs rpm. Effect of different image capture frequency for the set of experiments at C=T/5.

The total number (J=2000/f^{-1}) of selected images were used then to calculate the absolute difference between each consecutive selected images *j* and *j* +1. From the calculated image differences, each pixel with a grayscale value >10 was identified as a moving particle. This value was calculated from the variance of the distribution of greyscale values at the bottom of the vessel without particles, multiplied by the average value of greyscale in the cropped image.

The total amount (x_j) of moving particles was then identified for each image pair. Using the information acquired for the different pairs (number of pair =J-1), an average value of the total amount of moving particles was calculate ($\widetilde{x_J} = \sum_0^{J-1} x_j$). Using $\widetilde{x_J}$ and $\tilde{x}$, a $f_{\text{mov/tot}}$ parameter is defined as the ratio between the two calculated parameters ($f_{\text{mov/tot}} = \frac{\widetilde{x_J}}{\tilde{x}}$). This analysis was then performed for each set of data acquired for each experimental run (6 speeds [1000, 1200, 1400, 1600, 1800 and 2000 rpm] for each *C/T* value [1/3, 1/5, 1/7). All described steps were computed automatically for each set of data using a self-developed MATLAB script. The overall processing time was 10 minutes for the whole range of frequencies per run.

As can be seen in Fig. 3, the $f_{mov/tot}/f_{max}$ is sensitive to the frequency of capture:

I. At a low image capture frequency, there is a drastic increase of error in the data with the increase of rpm. This level of error suggests that at higher rpm, the particle movements cannot be captured properly at low frequency.

II. At very high frequency (above 400 Hz) for low rpm, it seems to underestimate the amount of moving particles. This outcome can be explained by estimating the minimum time for displacement (which is related to the particle speed generated by the impeller speed) as the particles move. This minimum time has been estimated as the ratio of the particle diameter divided by U_{tip}. According to the capture frequency then, it is possible to estimate the elapsed time between frames (f^{-1}). If the order of magnitude of elapsed time is smaller than the minimum time during which particles can be seen to move, their movements cannot be detected properly ("fake detection"). Following these considerations and comparing these minimum times and the elapsed times at different frequencies, all values above 400 Hz were considered not optimal. Moreover, observing the data for 400Hz and 2000Hz, this "fake detection" phenomenon can be observed happening for different range of speeds accordingly to the frequency (< 1400rpm for 400Hz and < 1600rpm for 2000Hz), where only the highest capture frequency can detect real movements at higher speeds.

III. Finally, it was observed that at higher and lower frequencies, when different phenomena (explained in the previous two points I and II above) were affecting the quality of the results, the distribution of standard deviations between runs was uneven. For the selected optimal frequency (100 Hz), the standard deviation for each data point at different rpm was low and consistent through the entire data set.

2.3.2. Computational Fluid Dynamics (CFD) simulation

To simulate the impeller rotation, either the sliding grid (SG) or multiple reference frame (MRF) approach has been used [45-48]. Although the SG approach is slightly more accurate, it requires higher computational power [46] and the MRF approach is able to provide acceptable simulation results, Therefore, the MRF approach was used to simulate the impeller rotation in this paper. In this case, the water near the impeller was taken as the moving zone, with the static zone elsewhere (impeller and shaft volume). In addition, whilst successively finer grids yield better simulation results [46, 49], it gives only a limited improvement for mean velocity profiles. Based on a grid independence study, a three-dimensional computational domain with 1100000 grids for the static zone and 400000 of non-uniform grids for the moving zone were used in each simulation. During the simulation, the impeller speed was fixed at 1000 rpm. The top of the tank was defined as a symmetry boundary condition. The impeller blades, disc, baffles, and tank walls were defined as 'non-slip' wall conditions and between the moving zone and the static zone, the interface was used for data transfer purposes. The standard k-ε turbulence model was used along with standard wall functions to account for the viscous flow region near the wall.

Simulations were performed by ANSYS FLUENT 16.1. The Pressure-Implicit with Splitting of Operators (PISO) algorithm was used for pressure-velocity coupling. The Pressure Staggering Option (PRESTO) was chosen for pressure interpolation scheme. The Quadratic Upwind Interpolation (QUICK) scheme was applied for the momentum, turbulent kinetic energy, and turbulent energy dissipation rate. The time step used in the simulations was 0.0001 s. Convergence was achieved when residuals on continuity, velocities, kinetic energy and energy dissipation rate became less than 10^{-4}. The simulations were conducted for 5 s in each simulation.

2.3.3. Particle Image Velocimetry (PIV)

The PIV test system is given in Fig. 1 b. The PIV apparatus (TSI Inc, USA) consists of a 532 nm (green) Nd-YAG laser (Litron Nano PIV) pulsing at 7 Hz, synchronized to a single TSI Power view 4MP (2048 × 2048 pixels^2) 12 bits CCD camera using a synchronizer (TSI 610035) attached to a personal computer.

The PIV system was controlled using TSI Insight 4G software. The tracer particles with diameter of 10 µm were added to the distilled water to capture the flow patterns with the laser plane passing through the center of the shaft in all measurements. The maximum separation, dT_{max}, is given as a function of the image magnification and the maximum velocity within the system [50].

$$dT_{max} = 0.25 L_{IA} M / U_{tip} \quad (1)$$

where M is image magnification (µm/pixel); U_{tip} is impeller tip velocity (m/s). L_{IA} is the side length of the interrogation window in pixels and was fixed at 32 in the tests. The PIV measurements were captured as time average data [51] from 500 instantaneous velocity fields using the MATLAB code.

2.3.4. Power consumption

The impeller power number, *Po*, for the difference clearances were calculated as follows [52]:

$$Po = \frac{2\pi NM}{\rho_l N^3 D^5} \quad (2)$$

where, *N* is the impeller speed, (m s^{-1}); *M* is the torque, (N · m), ρ_l is liquid density, (kg m^{-3}); D is impeller diameter, (m). 12 impeller speeds using water as continuous phase in the vessel have been used. For each experiment, three repeats were used to determine Po in the turbulent regime for each *C/T*. The torque measurement set up is shown in Fig. 1 d. The impeller shaft was connected to a Heidolph overhead stirrer equipped with a TorqSense RWT410 (1 mN) torque meter.

Power numbers were also estimated from the CFD analysis based on the torque balance over the impeller.

3. Results and Discussion

3.1. Particle suspension: Image analysis

The greyscale distribution of the horizontal plane of the tank bottom at different clearances and speeds are shown in Fig. 4. Each image represents an instantaneous time for the different configurations and rpm used. The general trends indicate that the pattern of the unsuspended particles changes with *C/T* and rpm as expected. Similar images were also obtained by Ibrahim and Nienow in a larger tank [34].

It is also interesting to focus on the variation of particle distribution with impeller speed in each clearance. At *C*=*T*/7, for example, increasing the impeller speed leads to a decrease in the number of particles settled at the tank bottom. Also, comparison of the images at 1000 rpm for the 3 clearances, shows that for the tank with impeller clearances, *C*=*T*/3 and *C*=*T*/5, as full suspension is approached with increasing impeller speed, particles are settled in the bottom center. On the other hand under similar conditions, particles are collected around the baffle in the tank with impeller clearance at *C*=*T*/7. In addition, less particles are identified near the bottom of the tank at *C*=*T*/7. Although no obvious difference of particle distribution is identified for *C*=*T*/3 and *C*=*T*/5, the images show that lowering the impeller clearance decreases the number of particles settled on the tank bottom. Averaging those images by the total amount of captured, which is related to the frequency of capture used, the average amount of unsuspended particles ($\tilde{x}$) is determined.

Figure 4. Greyscale distribution of horizontal plane of the bottom of the vessel at different clearances and speeds

For another demonstration of the particle distribution, a comparison of identified moving particles with impeller speeds at different clearances is also illustrated in Fig. 5. Comparing the moving particle distributions for each impeller clearance, it is apparent that the number of moving particles increases with impeller speed. In addition, focusing on the particle distribution at each clearance, lowering impeller speed makes the particles move homogeneously, especially for the clearance at C=T/7. Besides, the lower the impeller clearance, the more moving particles are identified. These results further imply that the particle suspension performance is improved with a lower impeller clearance.

Figure 5. Comparison of identified moving particles with impeller speeds at different clearances

3.2. Particle suspension: Quantitative results

The new defined parameter (See section 2.3.1, $f_{mov/tot}$, is defined as the fraction of number of moving particles ('any pixel not white' which has a grey scale value > 10) (Fig. 5) to the total amount of particle presented at the bottom of vessel ("yellow" pixels in Fig. 4). This parameter has been divided by the maximum value achieved in the set of experiments as a baseline for comparison between different runs. The highest value (f_{max}) has been obtained for the experimental condition when higher rpm and lower C/T were employed. Then the $f_{mov/tot}/f_{max}$ values have been plotted versus rpm to show quantitatively the different performance of the different configuration (varying *C/T* and *rpm*).

Figure 6. New parameter $f_{mov/tot}/f_{max}$ vs rpm. Effect of impeller clearance at selected image capture frequency (100 Hz).

As mentioned in Section 2.3.1 100 Hz was selected as the optimal frequency in order to compare the different set of experiments. To further illustrate the influence of impeller clearance on particle suspension, the variation in $f_{mov/tot}/f_{max}$ with impeller speed at the frequency of 100 Hz for each impeller clearance is presented in Fig. 6. In general, the $f_{mov/tot}/f_{max}$ increases with the impeller speed, especially for the $C = T/7$ case. The $f_{mov/tot}/f_{max}$ changes sharply when the impeller clearance decreases from $C = T/5$ to $C = T/7$. In contrast, lowering the impeller clearance from $C = T/3$ to $C = T/5$ has a minor increase on the $f_{mov/tot}$ for each speed. For the C = T/7 system, with the increase of impeller speed, the $f_{mov/tot}/f_{max}$ value increases before reaching a converged result. Further increase of the impeller speed above this critical speed has a minor effect on the $f_{mov/tot}/f_{max}$. N_{js} in this work has been defined as the speed at which $f_{mov/tot}/f_{max}$ is equal to 1. For the $C = T/7$ system, the N_{js} is approximately 1600 rpm. Further increase of impeller speed over 2000 rpm for the $C = T/3$ and $C = T/5$ system introduces lots of air. Thus, the limit speed without air, 2000 rpm, is regarded as the N_{js} for $C = T/3$ and $C = T/5$.

3.3. Particle suspension: Comparison with previous work

To validate the results obtained with the proposed new image analysis method, a comparison of N_{js} with previous work and with values obtained using the traditional visual approach is presented in Tab. 3. The results IN RELATION TO *C/T* obtained with the image analysis methodology, are in agreement with previous findings from different research groups [5, 33, 34, 37, 38, 41] and visual observations in this study. The N_{JS} values calculated from the work of Nienow [33] are very similar to values at the same *C/T* from other work (data not shown) [34, 41]. Where only one value is given it is because in the study of Armenante and co-workers [4], *C/T* = 1/7 was the highest value that they used; and in the earliest [5] and most recent work [40], clearance was not found to have any significant effect. Based on the information from the literature and the visual observations made at

the same time as shown in Tab. 3, it can be concluded that the proposed new image analysis method is able to measure N_{js} and the impact of clearance on it.

3.4. Validation of flow patterns using CFD and PIV analysis

To further investigate the reason for the effect of clearance on the particle suspension, CFD simulation and PIV experiments were used. In particular, flow patterns in the stirred tank were measured in the single phase system by PIV and used to validate those predicted by CFD as the impeller clearance was varied. Then the 3D information obtained from CFD simulation was additionally used to determine the distribution of strain rate at the bottom of vessel.

The normalized mean velocity between the numerical analysis and experimental measurement was used to check the validity of the CFD simulations [53, 54]. Fig. 7 shows the axial profiles of the normalized radial and axial component velocity near the impeller for $C = T/3$ at 1000 rpm. As can be seen, the CFD simulation results are closely comparable with the PIV measurements. Some of the values do not overlap perfectly but this is due to the different discretization used for the CFD simulations and raw PIV data treatment in addition to the inevitable slight difference in geometry between the 'ideal' shape of that simulated and the actual shape of the equipment.

Figure 7. Comparison between PIV and CFD results at C=T/3, N=1000 rpm: Location of line comparison: x/T=0.2 and between y/H=0.25 to y/H=0.45 (a); Normalised radial component velocity distribution U_x/U_{tip} (b); Normalised axial component velocity distribution U_y/U_{tip} (c).

The good agreement between the CFD and the PIV results is also indicated by the overall mean flow fields compared in Fig. 8. Here, the contour plots (PIV) and streamlines plot (CFD) are shown for the three different impeller clearances at 1000 rpm. As it can be seen, the CFD velocity streamlines match very well the PIV measurements. In fact, the double loop flow patterns are established above and below the impeller for $C = T/3$ and $C = T/5$ configurations both in the CFD modelling data and in the PIV measurements. However, for the $C=T/7$ case, only one single loop is established near the tank bottom in accordance with many earlier observations [5, 33, 38].

Figure 8. CFD simulation and PIV measurements: vertical planes for each clearance at 1000 rpm

Using the 3D information from the CFD simulation, it is also interesting to consider the distribution and magnitude of the strain rate at the bottom of the vessel. By examining the strain rate distribution occupying a 2 mm thin layer along the tank bottom (Fig. 9a), the strain rate contour map at the base at 1000 rpm for each impeller clearance (illustrated in Fig. 9b) can be obtained. As can be, seen, a high strain rate exists near the centre of the tank bottom for the $C = T/7$ clearance, which prevents particles settling in that region as observed in the images of Fig. 4.

Figure 9. Volume comparison location at the bottom of the tank with a thickness of 2 mm (a) and strain rate contour map at 1000 rpm (b)

Furthermore, the cumulative fraction of strain rate at bottom of the tank for different impeller clearances at 1000 rpm is plotted in Fig. 10. As shown in Fig.9, higher and more distributed values of rate of strain are present for the lower *C/T* in the entire volume of the tank. This implies that the strain rate increases as the impeller clearance decreases. Besides, as shown in Fig. 10, the strain rate near the bottom of the tank with impeller clearance of *C = T*/7 is far larger than that at *C = T/*3 and *C = T/5*. These strain rate plots show that lowering impeller clearance strengthens the strain rate near the tank bottom, which provide more energy to suspend the particles.

3.5 Power numbers

The *Po* numbers for each *C/T* obtained experimentally were close to the expected value of 5. However, the differences between the *Po's* at different *C/T* were smaller than the standard deviation of the acquired data, so no strong conclusions could be made. In the CFD analysis, *Po* at *C/T* = 1/7 with a single flow loop compared to *C/T* = 1/3 with a double loop was 15% lower in the former case and 20% lower in the latter, a trend in agreement with the literature.

Figure 10. Cumulative plot of strain rate near the bottom for different impeller clearances at 1000 rpm

4. Conclusions

A new quantitative methodology is presented for measuring particles suspension characteristics; it is more objective than the usual method which relies on visual observation. A comparison of the effect of impeller clearance on N_{js} with this new quantitative method with predictions from previous studies and visual observation during this one shows good agreement. In addition, fluid flow information from PIV and CFD have been used to help explain the suspension findings. The main conclusions can be drawn as follows:

(1) The transformation from raw image to greyscale image for further quantitative assessment of particle suspension is effective. It also shows that the number of moving particles increases and static ones decreases with increasing impeller speed.

(2) Lowering the impeller clearance improves the particle suspension performance in general and the impeller speed required for particles suspension at *C = T*/7 is much less than at *C = T*/3 **and** *C = T/5*.

(3) The CFD modelling also shows that at any given speed, the strain rate near the tank bottom rises.

(4) Both PIV and CFD show that lowering impeller clearance leads to a flow pattern transformation from a double to a single loop. The CFD and torque measurement also show that this transition is associated with the power number falling. The lower power number and the lower speed at the lowest clearance combine to give an enhanced reduction in mean specific energy dissipation rate compared to the higher clearance with double loops as found earlier [41].

Acknowledgments

Special thanks to the School of Chemical Engineering at University of Birmingham (UK) for supporting this work. This research did not receive any specific grant from funding agencies in the public, commercial, or not-for-profit sectors.

Symbols

C	[m]	Impeller clearance
D	[m]	Impeller diameter
J	[-]	Total number of selected images
H	[m]	Depth of liquid
L_{IA}	[pixel]	Side length of interrogation window
M	[N · m]	Torque
M	[µm/pixel]	Image magnification
N	[m/s]	Impeller speed
N_{js}	[rpm]	Minimum impeller speed
N_p	[-]	Power number
T	[m]	Tank diameter
U_{tip}	[m/s]	Impeller tip velocity
U_x	[m/s]	Radial component velocity
U_y	[m/s]	Axial component velocity
W	[m]	Baffle width (four baffles)
a	[m]	Impeller blade width
b	[m]	Shaft diameter
d	[m]	Disk diameter
dT_{max}	[s]	Maximum separation time
e	[m]	Impeller blade thickness
f	Hz	Image frequency
j	[-]	Selected image
$f_{mov/tot}$	[-]	Ratio of mean number of moving particles to total number of particles
h	[m]	Impeller blade height
w_{solid}/ w_{liquid}	[-]	Solid concentration
$\tilde{x}$	[-]	Average amount of un-suspended particles
$\tilde{x}_J$	[-]	Total amount of moving particles
x_j	[-]	Amount of moving particles for each image difference
ρ_L	[kg/m^3]	Fluid density
μ_L	[mPa·s]	Fluid viscosity
ρ_T	[kg/m^3]	Tracer particle density

d_p	[mm]	Diameter of glass particles
ρ_P	[kg/m^3]	Density of glass particles

References

[1] A. Nienow, K. Coopman, T. Heathman, Q. Rafiq, C. Hewitt, in Stem Cell Manufacturing, (Eds: J. M. S. Cabral, C.L. de Silva, L. G. Chase, d. M. M. Diogo), Elsevier Science, Cambridge, USA, 2016, 43-75.

[2] A. W. Nienow, The Canadian Journal of Chemical Engineering, 1969, (47), 248-258. DOI: 10.1002/cjce.5450470316

[3] A. W. Nienow, E. L. Paul, Wiley-Interscience, New York, USA, 2016, 665-728.

[4] T. N. Zwietering, Chemical Engineering Science, 1958, 8, 244-253. DOI: 10.1016/0009-2509(58)85031-9

[5] P. M. Armenante, E. U. Nagamine, Chemical Engineering Science, 1998, 53 (9), 1757-1775. DOI: 10.1016/S0009-2509(98)00001-3

[6] L. Liu, M. Barigou, International Journal of Multiphase Flow, 2015, 73, 80-89. DOI: 10.1016/j.ijmultiphaseflow.2015.03.008

[7] P. J. Ferreira, M. G. Rasteiro, M. M. Figueiredo, Advanced Powder Technology, 1994, 5 (1), 15-24. DOI: 10.1016/S0921-8831(08)60621-4

[8] H. Yamazaki, K. Tojo, K. Miyanami, Powder Technology, 1986, 48 (3), 205-216. DOI: 10.1016/0032-5910(86)80043-2

[9] M. V. Sardeshpande, G. Kumar, T. Aditya, V. V. Ranade, Flow Measurement and Instrumentation, 2016, 47, 110-121. DOI: 10.1016/j.flowmeasinst.2016.01.003

[10] G. Li, Z. Li, Z. Gao, J. Wang, Y. Bao, J. J. Derksen, Chemical Engineering Science, 2018, 191, 288-299. DOI: 10.1016/j.ces.2018.06.073

[11] L. Fan, N. Xu, Powder Technology, 2017, 316, 329-337. DOI: 10.1016/j.powtec.2016.10.065

[12] P. Guiraud, J. Costes, J. Bertrand, Chemical Engineering Journal, 1997, 68 (2-3), 75-86. DOI: 10.1016/S1385-8947(97)00076-4

[13] I. Ayranci, S. M. Kresta, Chemical Engineering Research and Design, 2014, 92 (3), 413-422. DOI: 10.1016/j.cherd.2013.09.005

[14] Narayana.S, V. K. Bhatia, D. K. Guha, M. N. Rao, Chemical Engineering Science, 1969, 24 (2), 223-&. DOI: 10.1016/0009-2509(69)80031-X

[15] A. Brucato, V. Brucato, Can J Chem Eng, 1998, 76 (3), 420-427. DOI: 10.1002/cjce.5450760311

[16] D. Guha, P. A. Ramachandran, M. P. Dudukovic, Chemical Engineering Science, 2007, 62 (22), 6143-6154. DOI: 10.1016/j.ces.2007.06.033

[17] A. Tamburini, A. Cipollina, G. Micale, A. Brucato, M. Ciofalo, Chemical Engineering Journal, 2012, 193-194, 234-255. DOI: 10.1016/j.cej.2012.04.044

[18] R. Jafari, P. A. Tanguy, J. Chaouki, International Journal of Chemical Engineering, 2012, 2012, 1-15. DOI: 10.1155/2012/945314

[19] M. Bohnet, G. Niesmak, Distribution of solids in stirred suspensions, 1980. Ger. chem. Eng, 3, p. 57

[20] L.Musil;, J. V. Jiroudková, Chemical Engineering Science, 1984, 39 (4), 621-628. DOI: 10.1016/0009-2509(84)80168-2

[21] C.Buurman;, G.Resoort;, A.Plaschkes, Chemical Engineering Science, 1986, 41 (11), 2865-2871. DOI: 10.1016/0009-2509(86)80017-3

[22] V. B. Rewatkar ; , K. S. M. S. Rao ; , J. B. Joshi, Industrial & Engineering Chemistry Research, 1991, 30, 1770-1784. DOI: 10.1021/ie00056a013

[23] M. Kraume, Chemical Engineering Technology, 1992, 15, 313-318. DOI: 10.1002/ceat.270150505

[24] A. Mersmann, F.Werner, S.Maurer, K.Bartosch, Chemical Engineering and Processing, 1998, 37, 503-510. DOI: 10.1016/S0255-2701(98)00057-9

[25] G. Micale, V. Carrara, F. Grisafi, A. Brucato, Chemical Engineering Research and Design, 2000, 78 (3), 319-326. DOI: 10.1205/026387600527374

[26] Y. Zhu;, J. Wu, The Canadian Journal of Chemical Engineering, 2002, 80 (4), 1-6. DOI: 10.1002/cjce.5450800417

[27] T. Jirout, J. Moravec, F. E. Rieger, V. Sinevič, M. Špidla, V. Sobolík, J. Tihon, Electrochemical measurement of impeller speed for off-bottom suspension, 2005.

[28] R. Congjing;, J. Xiaojing;, W. Jingdai;, Y. Yongrong;, Z. Xiaohuan, Industrial & Engineering Chemistry Research, 2008, 47 (15), 5323-5327. DOI: 10.1021/ie0714347

[29] A. Brucato, A. Cipollina, G. Micale, F. Scargiali, A. Tamburini, Chemical Engineering Science, 2010, 65 (10), 3001-3008. DOI: 10.1016/j.ces.2010.01.026

[30] S. M. Naghavi, On Lattice Boltzmann flow simulations in Stirred Tanks, 2010.

[31] B. Blais, O. Bertrand, L. Fradette, F. Bertrand, Chemical Engineering Research and Design, 2017, 123, 388-406. DOI: 10.1016/j.cherd.2017.05.021

[32] B. Blais, M. Lassaigne, C. Goniva, L. Fradette, F. Bertrand, Journal of Computational Physics, 2016, 318, 201-221. DOI: 10.1016/j.jcp.2016.05.008

[33] A. W. Nienow, Chemical Engineering Science, 1968, 23 (12), 1453-1459. DOI: 10.1016/0009-2509(68)89055-4

[34] S. Ibrahim, A. W. Nienow, Chemical Engineering Research & Design, 1996, 74 (6), 679-688.

[35] S. Ibrahim, A. W. Nienow, Chemical Engineering Research & Design, 1995, 73, 485-491.

[36] G. Montante, K. C. Lee, A. Brucato, M. Yianneskis, Comput Chem Eng, 2001, 25 (4-6), 729-735. DOI:10.1016/S0098-1354(01)00648-2.

[37] A. Ochieng, M. S. Onyango, A. Kumar, K. Kiriamiti, P. Musonge, Chemical Engineering and Processing: Process Intensification, 2008, 47 (5), 842-851. DOI: 10.1016/j.cep.2007.01.034.

[38] P. M. Armenante, E. U. Nagamine, J. Susanto, Can J Chem Eng, 1998, 76 (3), 413-419. DOI: 10.1002/cjce.5450760310

[39] R. K. Grenville, A. T. C. Mak, D. A. R. Brown, Chemical Engineering Research and Design, 2015, 100, 282-291. DOI: 10.1016/j.cherd.2015.05.026

[40] R. K. Grenville, J. J. Giacomelli, D. A. R. Brown, Chemical Engineering Research and Design, 2016, 109, 730-733. DOI: 10.1016/j.cherd.2016.03.024

[41] C. M. Chapman, PhD Thesis, University of London, 1981.

[42] I. Ayranci, M. B. Machado, A. M. Madej, J. J. Derksen, D. S. Nobes, S. M. Kresta, Chemical Engineering Science, 2012, 79, 163-176. DOI: 10.1016/j.ces.2012.05.028

[43] Y. Zhang, Z. Zhang, C. Wei, H. Wang, Chinese Journal of Chemical Engineering, 2018, 26 (6), 1423-1429. DOI: 10.1016/j.cjche.2018.04.026

[44] A. W. Nienow, D. Miles, Chemical Engineering Journal, 1978, 15 (1), 13-24.

[45] A. Tamburini, A. Cipollina, G. Micale, A. Brucato, M. Ciofalo, Chemical Engineering Journal, 2013, 223, 875-890. DOI: 10.1016/j.cej.2013.03.048

[46] D. Wadnerkar, M. O. Tade, V. K. Pareek, R. P. Utikar, Particuology, 2016, 29, 16-33. DOI: 10.1016/j.partic.2016.01.012

[47] D. Wadnerkar, R. P. Utikar, M. O. Tade, V. K. Pareek, Advanced Powder Technology, 2012, 23 (4), 445-453. DOI: 10.1016/j.apt.2012.03.007

[48] V. Santos-Moreau, L. Brunet-Errard, M. Rolland, Chemical Engineering Journal, 2012, 207-208, 596-606. DOI: 10.1016/j.cej.2012.07.020

[49] N. Qi, H. Zhang, K. Zhang, G. Xu, Y. Yang, Particuology, 2013, 11 (3), 317-326. DOI: 10.1016/j.partic.2012.03.003

[50] A. Gabriele, A. N. Tsoligkas, I. N. Kings, M. J. H. Simmons, Chemical Engineering Science, 2011, 66 (23), 5862-5874. DOI: 10.1016/j.ces.2011.08.007

[51] F. Alberini, L. Liu, E. H. Stitt, M. J. H. Simmons, Chemical Engineering Science, 2017, 171, 189-203. DOI: 10.1016/j.ces.2017.05.034

[52] F. Scargiali, A. Tamburini, G. Caputo, G. Micale, Chemical Engineering Research and Design, 2017, 123, 99-110. DOI: 10.1016/j.cherd.2017.04.035

[53] D. A. Deglon, C. J. Meyer, Minerals Engineering, 2006, 19 (10), 1059-1068. DOI: 10.1016/j.mineng.2006.04.001

[54] Z. Chara, B. Kysela, J. Konfrst, I. Fort, Applied Mathematics and Computation, 2016, 272, 614-628. DOI: 10.1016/j.amc.2015.06.044

Figures

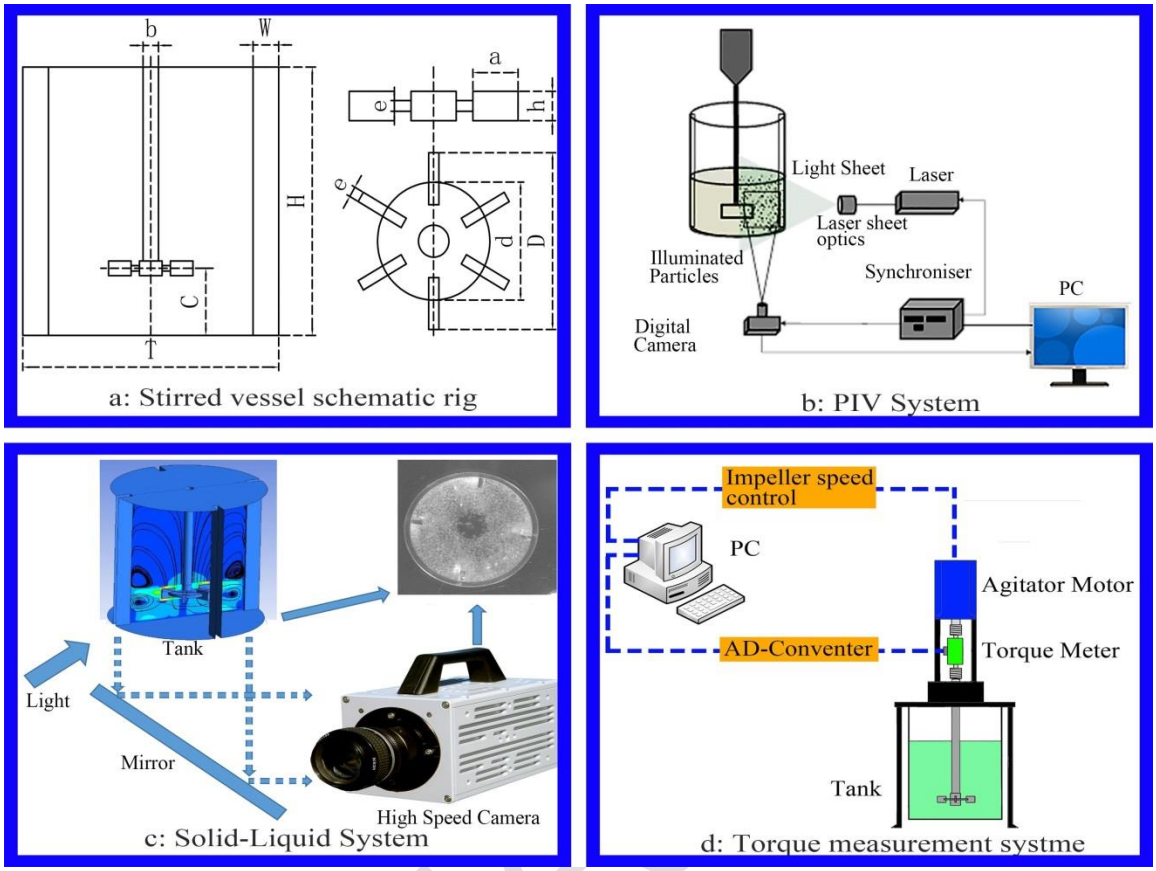

Figure 1. Experimental set-up

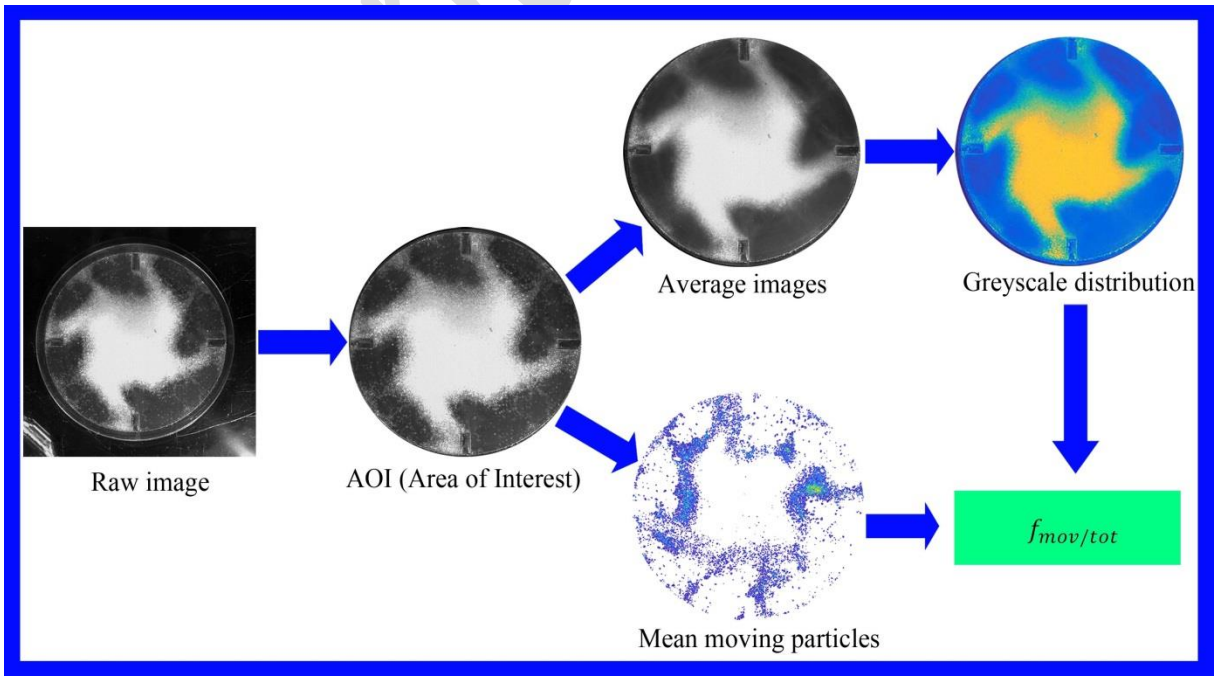

Figure 2. Image processing procedure

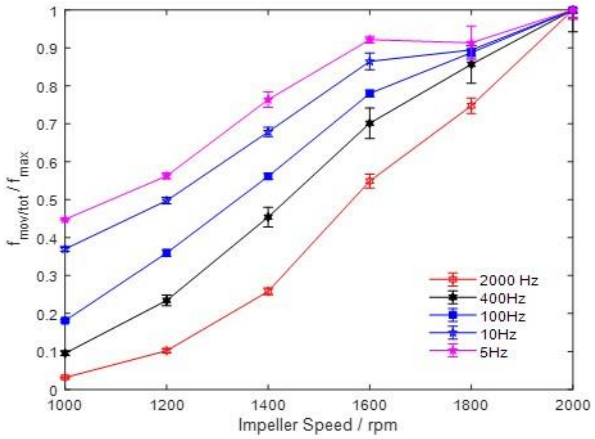

Figure 3. New parameter $f_{mov/tot}/f_{max}$ vs rpm. Effect of different image capture frequency for the set of experiments at C=T/5.

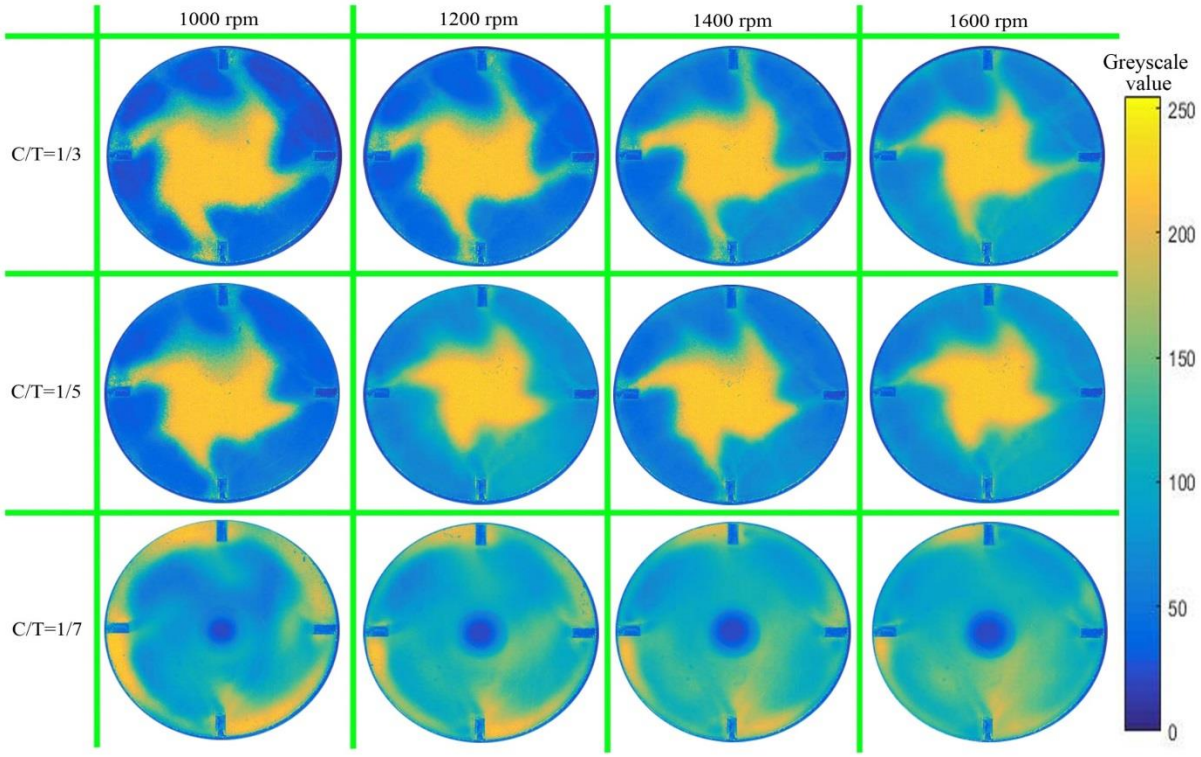

Figure 4. Greyscale distribution of the horizontal plane of the bottom of the vessel at different clearances and speeds

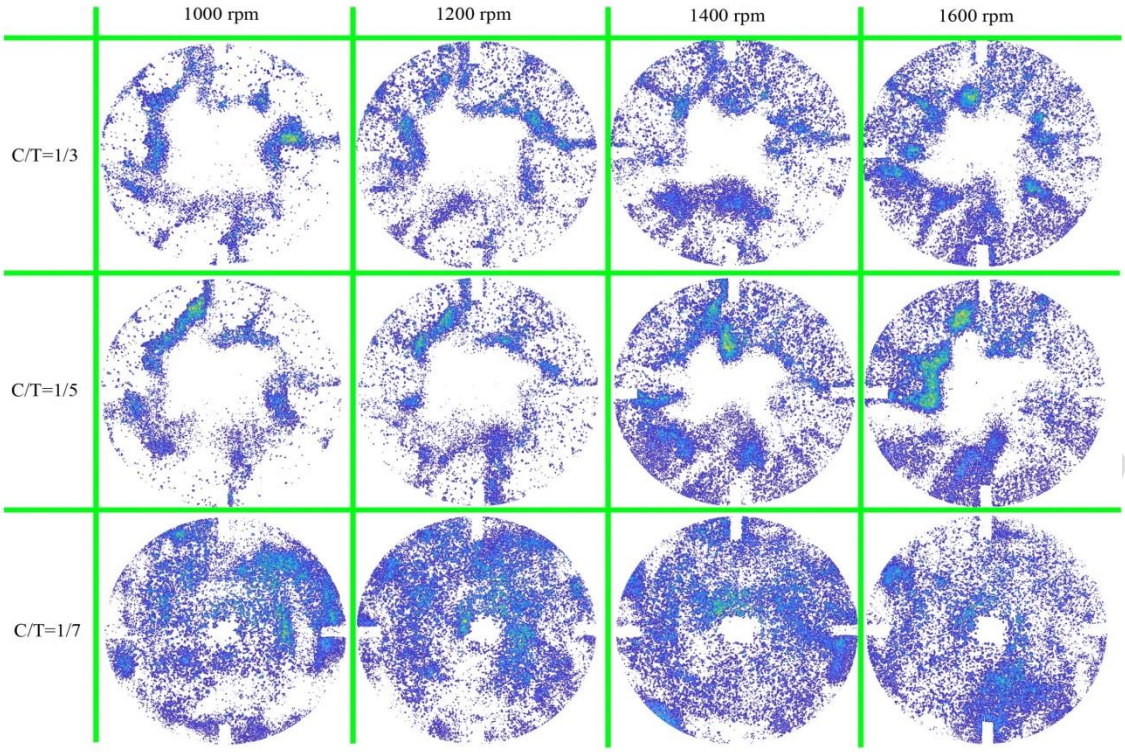

Figure 5. Comparison of identified moving particles with impeller speeds at different clearances

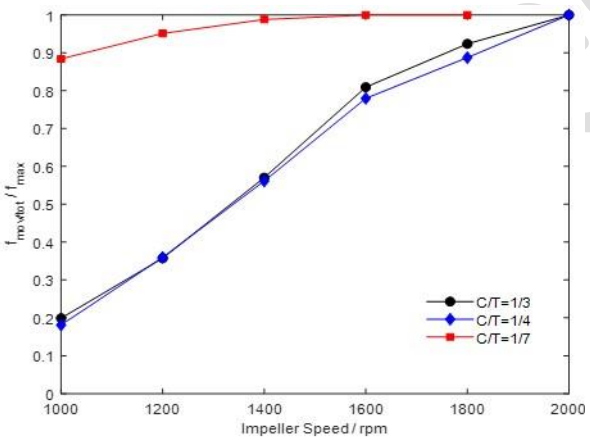

Figure 6. New parameter $f_{mov/tot}/f_{max}$ vs rpm. Effect of impeller clearance at selected image capture frequency (100 Hz)

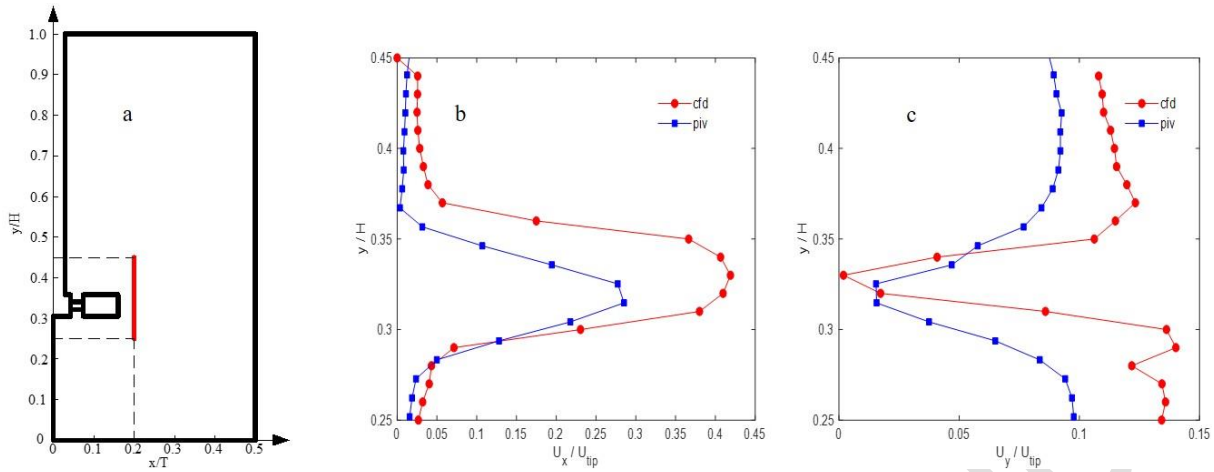

Figure 7. Comparison between PIV and CFD results at C=T/3, N=1000 rpm: a) Location of line comparison: x/T=0.2 and between y/H=0.25 to y/H=0.45; (b) Normalised radial component velocity distribution U_x/U_{tip}; (c); Normalised axial component velocity distribution U_y/U_{tip}.

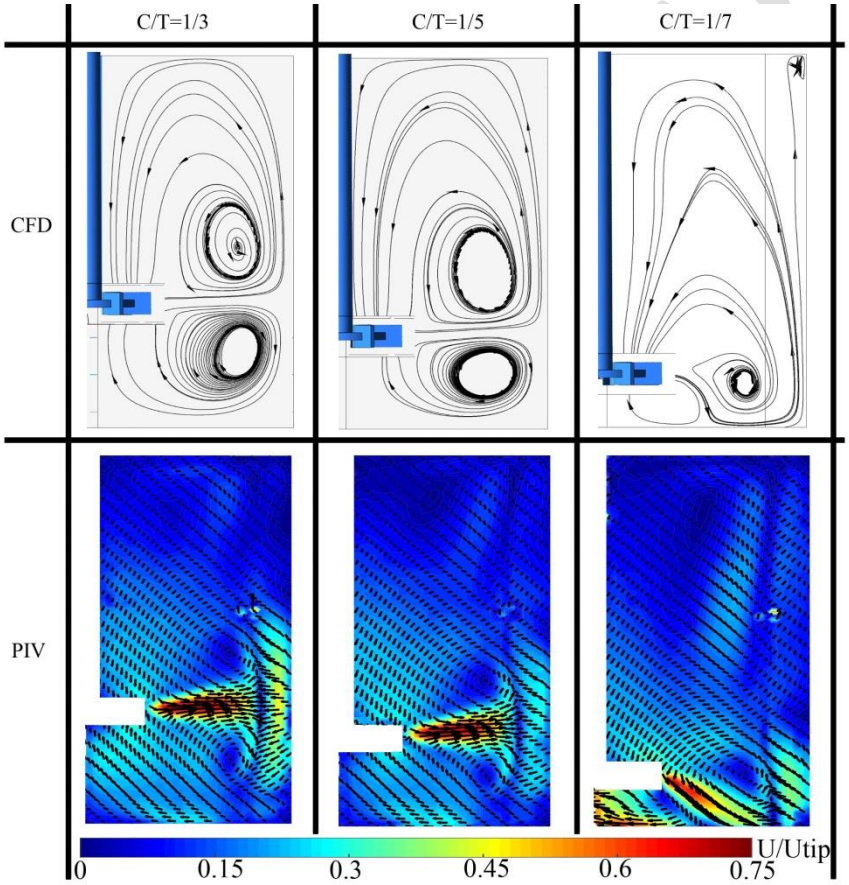

Figure 8. CFD simulation and PIV measurements: vertical planes for each clearance at 1000 rpm.

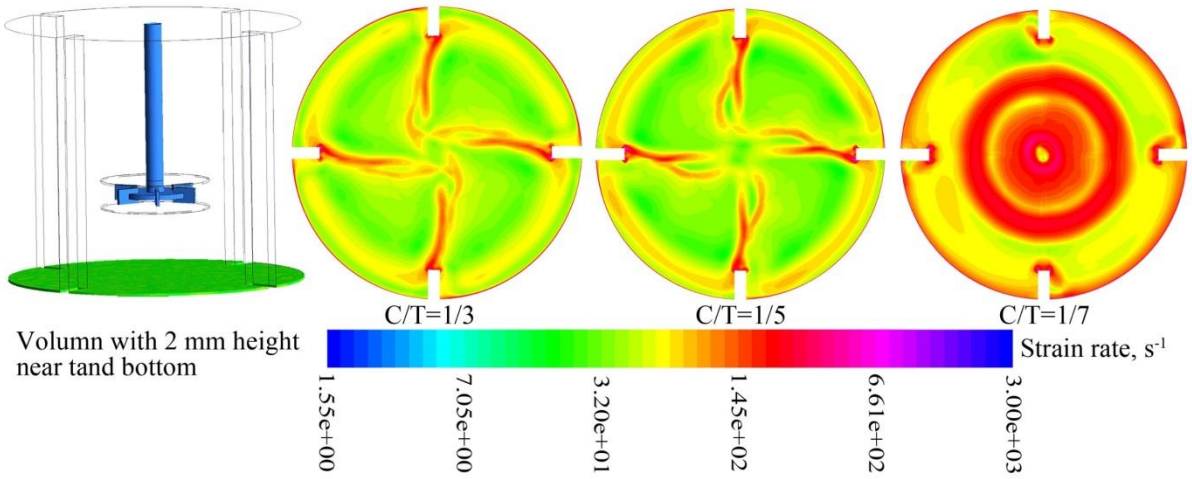

Figure 9. a) Volume comparison location at the bottom of the tank with a thickness of 2 mm; and (b) strain rate contour map at 1000 rpm.

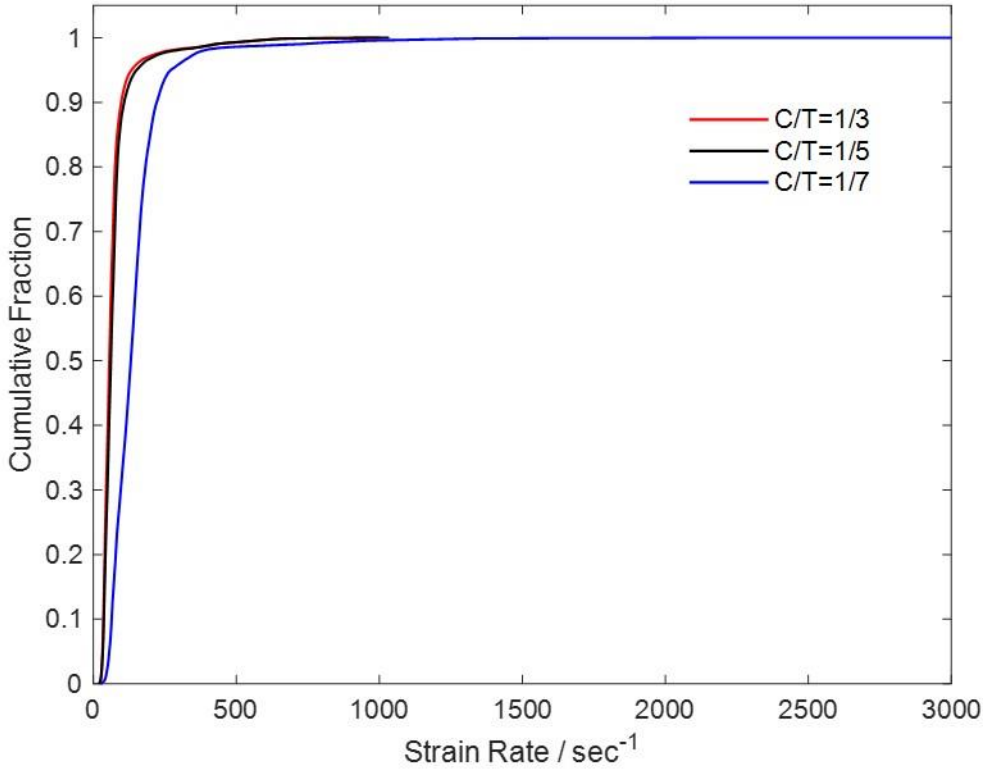

Figure 10. Cumulative plot of strain rate near the bottom for different impeller clearances at 1000 rpm

Tables

Table 1. Summary of experimental methods for characterizing Njs

method name	year	The criterion of N_{js} identification	Drawbacks
Zwietering [4]	1958	Particles settle down the tank bottom less than 1~2 sec	Only for low solid concentration system; high error;
Variation coefficient[19]	1980	Variation coefficient is 0.8.	Difficult to obtain the variation coefficient for different systems
Solid concentration [20]	1984	Discontinuity in solid concentration near the tank bottom	Intrusive, challenging concentration measurement
Velocity [21]	1985	The velocity near the tank bottom changes sharply	Large error; challenging operation
Power number [22]	1991	N_p remains constant with N	Measurement complex; lack generality;
Mixing time [22]	1991	N_{js} was noted from the curve of Mixing time with impeller speed	Mixing time measurement is challenging, not applicable for large-scale vessels
Radioactive tracer[22]	1991	The count rate suddenly dropped and remained practically constant	Expensive; detector position should be chosen carefully
Cloud height[23]	1992	Cloud height reached 90% of the total liquid height.	Not available for small particles or broad particle size distribution
Slurry height[24]	1998	No increase of slurry height with impeller speed	Hard to identify the slurry because of the vanishing interface
Pressure Gauge Technique[25]	2000	Calculated based on the variation in pressure with impeller speed	Complex, eliminating the effect of dynamic pressure head is empirical
Particle bed height[26]	2002	Solids bed height is zero	Difficult to verify the zero position
Electrochemical[27]	2005	The slopes of curves begin to decrease sharply	Hard to place the probe to the place of the last particles suspension
Acoustic Emission[28]	2008	Microscale energy fraction versus N occurs an abrupt slope	Signal processing method based on Multiscale Analysis is complex.
Steady Cone Radius [29]	2010	Steady cone radius shrinks to zero	Especially for unbaffled stirred tanks.
Gamma-ray densitometry[18]	2012	Gamma-ray intensity reaches a converged result	Expensive; Safety problem needs a careful consideration

Table 2. Stirred vessel schematic rig: C-Impeller clearance; D-Impeller diameter; H- Depth of liquid; T-Tank diameter; W-Baffle width (four baffles); a- Impeller blade width; b-Shaft diameter; d-Disk diameter; e- Impeller blade thickness; h- Impeller blade height

H/T	C/T	W/T	b, mm	T, mm	D/T	d/D	a/D	h/D	e, mm
1	1/3,1/5,1/7	1/10	6	100	1/3	3/4	1/5	1/5	2

,

Table 3. Comparison of Njs between literature and experiment

C/T	N_{js}, rpm					
	Visual experiment	Zwietering [4]	Nienow [33]	Armenante [5]	Grenville [40]	**Image analysis**
1/3	~2000		2384	—	—	**2000**
1/5	~2000	2027	1973	—	1913	**2000**
1/7	1500		1726	1589	—	**1600**